Ab initio and semiempirical modeling of excitons and trions in monolayer TiS_3

E. Torun,[1,2,*] H. Sahin,[3,4] A. Chaves,[5,6,†] L. Wirtz,[2] and F. M. Peeters[1]
[1]*Department of Physics, University of Antwerp, Groenenborgerlaan 171, 2020 Antwerp, Belgium*
[2]*Physics and Materials Science Research Unit, University of Luxembourg, 162a Avenue de la Faïencerie, L-1511 Luxembourg, Luxembourg*
[3]*Department of Photonics, Izmir Institute of Technology, 35430 Izmir, Turkey*
[4]*ICTP-ECAR Eurasian Center for Advanced Research, Izmir Institute of Technology, 35430 Izmir, Turkey*
[5]*Departamento de Física, Universidade Federal do Ceará, Campus do Pici, CP 6030, CEP 60455-900, Fortaleza, Ceará, Brazil*
[6]*Department of Chemistry, Columbia University, 3000 Broadway, 10027 New York, New York, USA*

(Received 3 May 2018; revised manuscript received 24 July 2018; published 21 August 2018)

We explore the electronic and the optical properties of monolayer TiS_3, which shows in-plane anisotropy and is composed of a chain-like structure along one of the lattice directions. Together with its robust direct band gap, which changes very slightly with stacking order and with the thickness of the sample, the anisotropic physical properties of TiS_3 make the material very attractive for various device applications. In this study, we present a detailed investigation on the effect of the crystal anisotropy on the excitons and the trions of the TiS_3 monolayer. We use many-body perturbation theory to calculate the absorption spectrum of anisotropic TiS_3 monolayer by solving the Bethe-Salpeter equation. In parallel, we implement and use a Wannier-Mott model for the excitons that takes into account the anisotropic effective masses and Coulomb screening, which are obtained from *ab initio* calculations. This model is then extended for the investigation of trion states of monolayer TiS_3. Our calculations indicate that the absorption spectrum of monolayer TiS_3 drastically depends on the polarization of the incoming light, which excites different excitons with distinct binding energies. In addition, the binding energies of positively and the negatively charged trions are observed to be distinct and they exhibit an anisotropic probability density distribution.

DOI: 10.1103/PhysRevB.98.075419

I. INTRODUCTION

After the synthesis of graphene [1,2], layered materials have received a lot of interest in the field of condensed matter physics and materials science. Among the recently synthesized groups of layered materials are the transition metal trichalcogenides (TMTCs) which have a chemical formula MX_3, where M stands for a transition metal from group IV, V, or VI in the periodic table (e.g., Ti, Zr, or Nb) and X is a chalcogen atom (e.g., S, Se, or Te). TMTCs are a much less explored class of materials when compared with the extensively studied transition metal dichalcogenides (TMDCs), which are considered promising candidates for a next generation of flexible nanoelectronic devices due to their wide range of different properties [3–9].

One of the major differences between these two classes of materials is the crystal symmetry. Although both are layered materials in their bulk form in which the interaction between each monolayer is governed by the weak van der Waals (vdW) forces, their in-plane symmetries are remarkably distinct. TMDCs show hexagonal in-plane geometry which is symmetric along different lattice directions, while TMTCs have a reduced in-plane structural symmetry due to bundles of molecular chains in a trigonal prism form where the centers of the prisms are occupied by transition metal atoms along one of the lattice directions [10,11]. This quasi-one-dimensional property leads to strong anisotropy in the electronic and optical properties and opens up new possibilities for devices with anisotropic functionalities such as polarization sensitive photodetectors, polarized light emission, integrated digital inverters, and tunable Schottky barriers [12–23].

Among these recently synthesized TMTCs, TiS_3 in particular has been gaining interest due to its robust direct band gap, band gap range, electron mobility, and its anisotropic physical properties. For instance, in contrast to the layered TMDCs, TiS_3 exhibits a direct band gap in both monolayer and bulk form of about 1 eV. It is important to note that the band gap and its direct character depend very slightly on the thickness and the stacking order of the constituent layers [23–26]; it changes slightly on the other hand with the application of tensile stress to the material [27]. It has also been shown that TiS_3 transistors show very high electron mobility and the current-voltage characteristics exhibit strong nonlinearity [28,29].

Although there has been an increasing interest in TiS_3 monolayers, theoretical investigations of its electronic and optical properties are sparse. Therefore, in this work we investigate the effect of the anisotropic crystal structure of monolayer TiS_3 on its exciton and trion properties by using first-principles calculations and a Wannier-Mott model. The low-energy response of two-dimensional (2D) materials is governed by excitonic and trionic states, so a proper description of them is crucial regarding the possible device applications.

II. RESULTS

A. Excitons in a TiS_3 monolayer

The first step to calculate the absorption spectrum and the excitons of monolayer TiS_3 is to obtain the Kohn-Sham

*engin.torun@uni.lu
†andrey@fisica.ufc.br

wave functions and eigenvalues with density functional theory (DFT). For this purpose we use the QUANTUM ESPRESSO code[30] with an $8 \times 12 \times 1$ **k**-point sampling, 180 Rydbergs for the plane-wave energy cutoff, and approximately 40 a.u. vacuum distance between the periodically repeated layers. We used the Perdew-Burke-Ernzerhof (PBE) exchange-correlation functional [31] and norm-conserving pseudopotentials of Goedecker-Hartwigsen-Hutter-Teter type[32,33], where for Ti atoms semicore electrons ($3p$ and $4s$) are explicitly treated as valence electrons. According to our calculations, the optimized lattice constants of pristine single-layer TiS_3 are $a_1 = 4.97$ Å and $a_2 = 3.40$ Å which are close to the experimental in-plane lattice parameters of bulk TiS_3 ($a_1 = 4.95$ Å and $a_2 = 3.40$ Å) [10,11].

In order to cure the intrinsic band gap underestimation problem of the Kohn-Sham DFT, we perform G_0W_0 [34,35] calculations with the plasmon-pole approximation as implemented in the YAMBO code [36]. Once we have obtained the corrected electronic band gap, we use a "scissor operator" to correct the DFT band gap. With that, we calculate the optical spectra of monolayer TiS_3 solving the Bethe-Salpeter equation [37–39] (BSE) in the following form, in which the electron-hole pairs are used to express the electronic excitations:

$$(E_{c\mathbf{k}} - E_{v\mathbf{k}})A^S_{vc\mathbf{k}} + \sum_{\mathbf{k}'v'c'} \langle vc\mathbf{k}|K_{eh}|v'c'\mathbf{k}'\rangle A^S_{v'c'\mathbf{k}'} = \Omega^S A^S_{vc\mathbf{k}}, \quad (1)$$

where $E_{c\mathbf{k}}$ and $E_{v\mathbf{k}}$ are the quasiparticle energies of the valence- and the conduction-band states for the vertical electronic transitions, respectively. The $A^S_{vc\mathbf{k}}$ are the expansion coefficients of the excitons, Ω^S are the eigenenergies of the possible excitation energies, and K_{eh} is the interaction kernel between electron and hole. If the interaction between electron and hole was absent in the above equation, the K_{eh} term would drop out and the excitations would correspond to independent electron-hole pairs. The imaginary part of the dielectric function $[\epsilon(\hbar\omega) = \epsilon_1(\hbar\omega) + i\epsilon_2(\hbar\omega)]$. which is the optical absorption spectrum of the compound, can be calculated as

$$\epsilon_2(\hbar\omega) \propto \sum_S \left| \sum_{cv\mathbf{k}} A^S_{vc\mathbf{k}} \frac{\langle c\mathbf{k}|p_i|v\mathbf{k}\rangle}{(\epsilon_{c\mathbf{k}} - \epsilon_{v\mathbf{k}})} \right|^2 \delta(\Omega^S - \hbar\omega - \Gamma), \quad (2)$$

where $\langle c\mathbf{k}|p_i|v\mathbf{k}\rangle$ is the dipole matrix element which corresponds to the transition from the valence to the conduction bands. In order to mimic the experimental resolution, an energy broadening of $\Gamma = 0.05$ eV is used in the calculations. Similar to G_0W_0 calculations, the BSE calculations are performed using the YAMBO code [36]. We have tested that the low-energy optical spectrum of monolayer TiS_3 is converged with a $24 \times 36 \times 1$ **k**-point mesh and with inclusion of the upper four valence and first four conduction bands. In order to avoid the long-range interaction between the periodic adjacent layers along the vertical direction, a Coulomb cutoff (Cc) of the screened potential is used in both G_0W_0 and BSE steps.

The rectangular primitive unit cell of monolayer TiS_3 contains two titanium (Ti) and six sulphur (S) atoms; two of these S atoms are inner and the rest of them are the outer S atoms, as shown in Fig. 1(a). The monolayer structure is formed as a chain-like structure which contains trigonal prisms

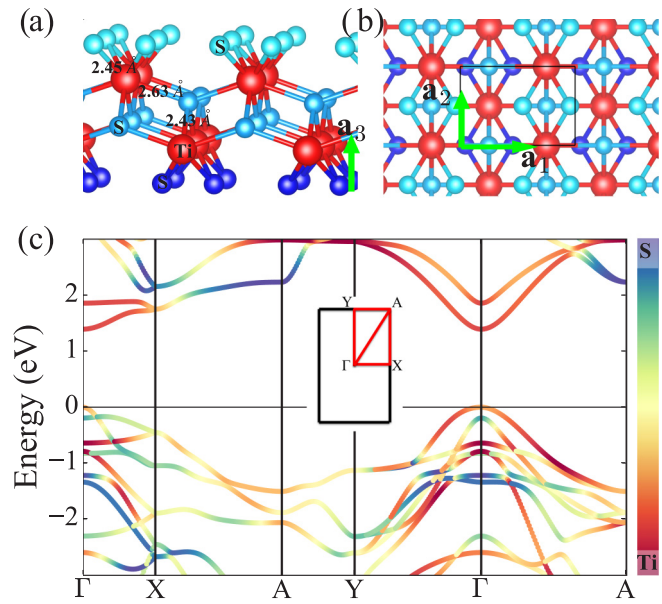

FIG. 1. The optimized geometric structure of monolayer TiS_3 [(a) and (b)]; the dark and the light blue balls represent the S atoms and the red ones represent the Ti atoms. The S atoms on different surfaces are colored differently for clarity, and the numbers in the figure are the bond lengths. The quasiparticle band structure of TiS_3 monolayer (c); the Brillouin zone (BZ) is shown in the inset of the figure. The in-plane ($\mathbf{a}_1$ and $\mathbf{a}_2$) and out-of-plane ($\mathbf{a}_3$) lattice vectors are also shown in the figure.

in which the metal atom occupies the center. The coordination of the atoms, the bond lengths, and the unit cell can be seen in Figs. 1(a) and 1(b); for clarity the outer and inner S atoms are shown in different colors in the figures. It is also worth mentioning that the Ti-S distance varies in the compound depending on the position of the bond in the structure. The anisotropy of the crystal structure along $\mathbf{a}_1$ and $\mathbf{a}_2$ directions is evident.

The quasiparticle band structure along the high symmetry points of the rectangular Brillouin zone (BZ) of monolayer TiS_3 is shown in Fig. 1(c). According to our DFT calculations, the TiS_3 monolayer has a direct band gap of 0.30 eV at the Γ point in the BZ, similar to the earlier PBE calculations [40,41]. As expected, the DFT gap is much smaller than the experimental electronic band gap and the optical band gap of TiS_3, which are reported to be around 1.2 and 1.1 eV, respectively [23–25]. Earlier calculations with the HSE06 hybrid functional reported the electronic band gap of monolayer TiS_3 as 1.05 eV [40], and GW calculations using the plasmon-pole approximation yielded around 1.15 eV [42,43]. It is important to mention that the inclusion of the Cc changes the converged electronic gap of pristine single-layer TiS_3. Using settings and pseudopotentials similar to the earlier studies, our calculations show that the band gap of TiS_3 monolayer becomes 1.2 and 1.4 eV without and with Cc, respectively. This is an expected result because Coulomb screening is larger if the Cc is not included in the calculation due to the extra screening which originate from the adjacent layers. The larger screening results in a smaller band gap than in the calculation with Cc, which cancels the interaction between the monolayer with its periodic image.

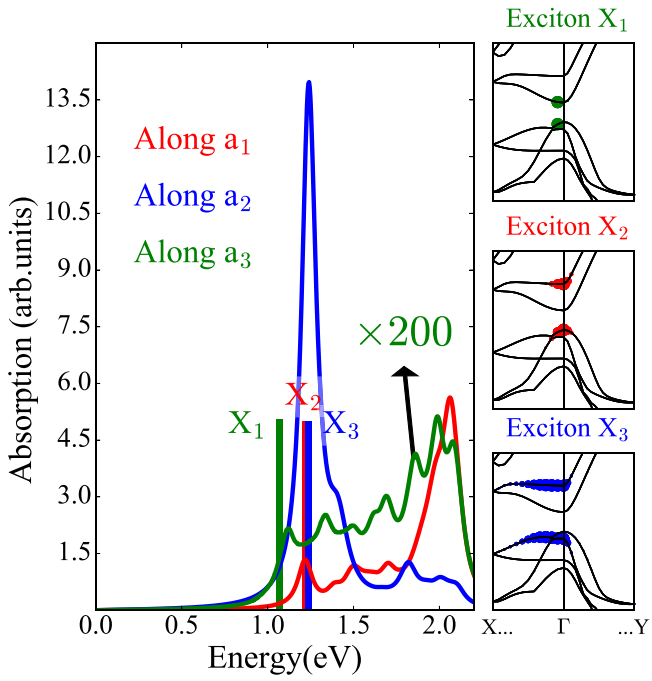

FIG. 2. Calculated absorption spectra of TiS_3 monolayer for different light polarization directions (direction of the electric field vector of light), in-plane ($\mathbf{a}_1$ and $\mathbf{a}_2$) and out-of-plane ($\mathbf{a}_3$), and the contributed states to the particular excitonic peak.

The main reason why the electronic band gap is closer to the experimental electronic band gap in the calculations without Cc is the effect of the dielectric substrate whose screening tends to reduce the band gap in experiments. Since we are dealing with an isolated single layer and Cc is essential to cancel the artificial interaction between monolayers, it is included in both the G_0W_0 and the BSE steps in our calculations. Therefore, in the BSE step the scissor operator is calculated considering the electronic band gap value obtained from the G_0W_0 calculation with Cc, which is 1.4 eV.

In Fig. 2, we present the absorption spectra of TiS_3 monolayer for different polarization directions, meaning that the electric field vector of the incoming light is along different orthogonal lattice vectors. The absorption spectra of pristine TiS_3 monolayer are remarkably different for different polarization directions due to the crystal anisotropy. Earlier theoretical works also predicted the polarization dependent absorption spectra of bulk TiS_3, but did not investigate the band composition responsible for the peaks in their absorption spectra [24,43]. In Fig. 2, the first bright excitons of each polarization direction are indicated in the figure as red, blue, and green colors for $\mathbf{a}_1$, $\mathbf{a}_2$, and $\mathbf{a}_3$ polarization directions, respectively. The excitonic state, which is due to the transition from the valence band maximum (VBM) to the conduction band minimum (CBM), is dark for in-plane polarizations (electric field vector of light is along $\mathbf{a}_1$ and $\mathbf{a}_2$) but it is bright for the out-of-plane polarization (electric field vector of light is along $\mathbf{a}_3$). The spectral position of the first excitonic peak is at 1.07 eV for the out-of-plane polarization direction, which is actually close to the optical gap of multilayer TiS_3 [24]. As expected, the absorption for out-of-plane polarization is small compared with the in-plane polarization absorption. Therefore, the absorption spectrum of the out-of-plane polarization direction was multiplied with a factor of 200 in order to provide a better visibility. The first bright excitons for the in-plane polarization directions are not from the VBM to CBM but from other bands around Γ, as shown in the same figure. Therefore, these excionic peaks are higher in energy than the exciton, which corresponds to the optical gap of the single-layer TiS_3. Another important conclusion that can be drawn from our calculations is that, depending on the polarization of the light, different excitons with different binding energies are excited. The binding energies are calculated as 0.59, 0.68, and 0.32 eV along $\mathbf{a}_1$, $\mathbf{a}_2$, and $\mathbf{a}_3$ lattice directions, respectively.

B. Neutral and charged excitons

In this section, we explore the neutral and charged excitons of monolayer TiS_3 using a Wannier-Mott model and focus only on in-plane polarization directions for the incident light. Therefore, we investigate only excitons labeled as X_2 and X_3 in the previous section (see Fig. 2). The conduction band for both cases is the same, with effective masses $m_e^x = 12.07m_0$ and $m_e^y = 0.42m_0$ in the Γ-X and Γ-Y directions, respectively, where m_0 is the free electron mass. On the other hand, the effective masses corresponding to the valence band involved in the X_2 transition are $m_h^x = 0.36m_0$ and $m_h^y = 0.90m_0$, whereas $m_h^y = 0.25m_0$ and $m_h^x \gg m_h^y$ for X_3. In fact, the valence band involved in X_3 is basically flat in the Γ-X direction; therefore, we just choose a very high number for the effective mass in this direction (for practical purposes, we assume $m_h^x = 50m_0$). Once the effective masses of electrons and holes are known, one can estimate the binding energies of excitons in TiS_3 within the Wannier-Mott model, which can be compared to the BSE results in the previous section. The advantage of developing this more simplistic effective mass model, validated by the BSE ones, lies in its flexibility. This approach allows us to easily incorporate substrate screening effects in the binding energy calculations, as well as to investigate charged excitons (trions), as we demonstrate in detail further on.

The Wannier-Mott exciton binding energies are obtained by numerically solving the Schrödinger equation in the electron-hole relative coordinates $\vec{R} = \vec{r}_h - \vec{r}_e$, whose Hamiltonian reads [44]

$$H_{exc} = -\frac{1}{\mu_x}\frac{\partial^2}{\partial X^2} - \frac{1}{\mu_y}\frac{\partial^2}{\partial Y^2} + V(\sqrt{X^2+Y^2}), \qquad (3)$$

where $\mu^{x(y)} = (1/m_e^{x(y)} + 1/m_h^{x(y)})^{-1}$ is the anisotropic reduced effective mass in the x (y) direction, energies are written in units of the Rydberg energy, and distances are scaled to the Bohr radius. The electron-hole interaction potential in such a thin material undergoes screening by the TiS_3 monolayer, as well as screening by the substrate on which it is deposited, with static dielectric constants ϵ and ϵ_s, respectively. The interaction potential (assuming vacuum above the TiS_3 layer) is approximately [45–48]

$$V(R) = -\frac{2\pi}{(1+\epsilon_s)\rho_0}\left[H_0\left(\frac{R}{\rho_0}\right) - Y_0\left(\frac{R}{\rho_0}\right)\right], \qquad (4)$$

where H_0 and Y_0 are Struve and Neumann functions, respectively, $\rho_0 = D\epsilon/(1+\epsilon_s)$ is the screening length, and

$D = 8.89$ Å is the monolayer thickness, estimated to be the same as the interlayer distance. Anisotropy in the static dielectric function of bulk TiS_3 ($\epsilon_x = 14.99\epsilon_0$, $\epsilon_y = 10.53\epsilon_0$, $\epsilon_z = 6.29\epsilon_0$) is taken into account by a geometric average of its components, $\epsilon = \sqrt[3]{\epsilon_x\epsilon_y\epsilon_z}$ [49]. It is worth pointing out that the dielectric screening provided by the substrate induces not only a smaller screening length for the electron-hole interaction potential in Eq. (4), but also a quasiparticle gap renormalization and, possibly, modifications to the band curvatures and, consequently, effective masses. The latter may lead to corrections on the exciton and trion binding energies, which are neglected in our calculations as an approximation. The exciton Hamiltonian H_{exc} is discretized in a nonuniform mesh, within a finite difference scheme [44], and then numerically diagonalized to obtain the excitonic spectrum.

As for charged excitons (trions), the system must be described, in principle, by six coordinates, namely, (x, y) coordinates for each of the three particles involved. In this case, a different change of coordinates is proposed, in order to reduce the dimensionality of the problem (see, e.g., the Supplemental Material of Ref. [50]): we take $\vec{R}$ (with corresponding momentum $\vec{P}$) as the relative coordinate between an electron-hole pair, and $\vec{r}$ (with corresponding momentum $\vec{p}$) as the relative coordinate between the extra charge (extra electron or hole, for negatively or positively charged trions, respectively) and the center of mass of that first electron-hole pair. This leads to a trion Hamiltonian

$$H_{\pm} = \frac{P_x^2}{2\mu^x} + \frac{P_y^2}{2\mu^y} + \frac{p_x^2}{2\mu_t^x} + \frac{p_y^2}{2\mu_t^y} + V_{\pm}. \tag{5}$$

The plus (minus) sign stands for a positively (negatively) charged trion, where an extra hole h' (electron e') is added through the trion reduced mass $\mu_t^{x(y)} = (1/\mu^{x(y)} + 1/\bar{m}_h^{x(y)})^{-1}$ [$\mu_t^{x(y)} = (1/\mu^{x(y)} + 1/\bar{m}_e^{x(y)})^{-1}$]. Accordingly, a more general form of the interaction potential Eq. (4) must be provided:

$$\begin{aligned} V_- &= V_{eh}(\vec{r}_h - \vec{r}_e) + V_{eh}(\vec{r}_h - \vec{r}_{e'}) + V_{ee}(\vec{r}_e - \vec{r}_{e'}), \\ V_+ &= V_{eh}(\vec{r}_h - \vec{r}_e) + V_{eh}(\vec{r}_{h'} - \vec{r}_e) + V_{hh}(\vec{r}_h - \vec{r}_{h'}), \\ V_{ij} &= \frac{q_i q_j e^2}{2(\epsilon_1+\epsilon_2)\rho_0}\left[H_0\left(\frac{|\vec{r}_i - \vec{r}_j|}{\rho_0}\right) - Y_0\left(\frac{|\vec{r}_i - \vec{r}_j|}{\rho_0}\right)\right], \end{aligned} \tag{6}$$

where $q_{e(h)} = -(+)$ is the electron (hole) charge. Notice that this final four-dimensional form of the trion Hamiltonian is obtained by taking the center-of-mass terms of the overall Hamiltonian to be zero, since the potential, Eq. (6), does not depend on either the excitonic or electron-exciton center-of-mass coordinates chosen in our transformation.

Numerical diagonalization of the matrix representing the four-dimensional trion Hamiltonian, Eq. (5), discretized in finite differences, requires a high computational cost. Alternatively, as we are interested only in the trion ground state, we obtain it by evolving an arbitrary initial wave packet in imaginary time $\tau = it$ until convergence is reached. The potential and kinetic energy terms in the time evolution operator $U(\tau + \Delta\tau, \tau) = \exp(-H_{\pm}\Delta\tau/\hbar)$ are conveniently split into a series of exponentials [51–53],

$$U(\tau + \Delta\tau, \tau) \approx e^{-\frac{\Delta\tau}{2\hbar}V} e^{-\frac{\Delta\tau}{\hbar}T_1} e^{-\frac{\Delta\tau}{\hbar}T_2} \cdots e^{-\frac{\Delta\tau}{\hbar}T_N} e^{-\frac{\Delta\tau}{2\hbar}V}, \tag{7}$$

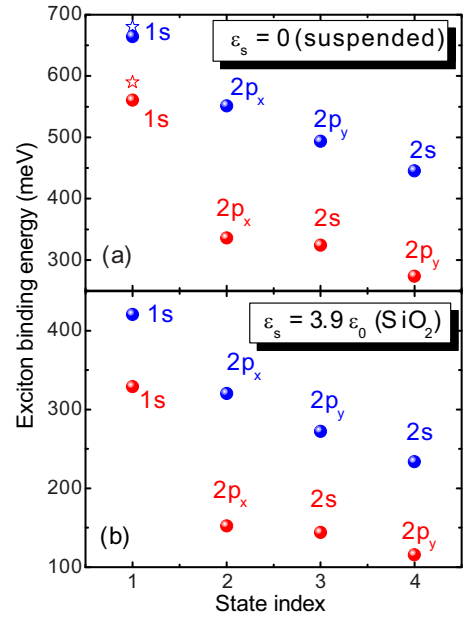

FIG. 3. Energy spectra of X_2 (red) and X_3 (blue) exciton states in monolayer TiS_3 in (a) the suspended case and (b) deposited over a SiO_2 substrate, along with the symmetry corresponding to each state, as calculated by the effective mass approach.

where T_i is the kinetic energy term in the i direction (for a system with N dimensions). This procedure requires lower computational cost, by paying the price of having a $O(\Delta\tau^3)$ error due to the noncommutativity between kinetic and potential operators, which is controlled here by using a small imaginary time step $\Delta\tau$. Finally, the resulting energy, obtained by the bra-ket of $H_{\pm}$ with the time-evolved wave function, is deducted from the exciton binding energy in order to obtain the trion binding energy $T_j^{\pm}$, with $j = 2, 3$ representing the type of exciton involved in this trion state.

The calculated binding energy of the X_2 (red) and X_3 (blue) excitons of monolayer TiS_3 are shown in Fig. 3 up to the third excited state, along with the symmetry of the corresponding wave functions of each state. High binding energies, of the order of hundreds of meV, are observed, which is a hallmark of 2D materials [54–59]. Besides, similar to, e.g., black phosphorus, which also exhibits strongly anisotropic bands, excitonic p states in monolayer TiS_3 are found to be nondegenerate, a feature that can be experimentally probed by two-photon absorption [60], while the degeneracy between s and p states is lifted by the non-Coulombic form of the electron-hole potential [44]. Results are shown for the suspended case [Fig. 3(a)] and for the case of TiS_3 over SiO_2 where $\epsilon_s = 3.9\epsilon_0$ [Fig. 3(b)]. In the former, we verify that the BSE results (open star symbols) are very close to the Wannier-Mott ones (full symbols), which helps to validate our model. Binding energies in the latter are significantly reduced by the additional dielectric screening provided by the substrate, but the ground state energy is still found to be as high as 330 and 421 meV for X_2 and X_3, respectively.

Figure 4 shows how the exciton and trion binding energies depend on the effective dielectric constant of the substrate ϵ_s. The trion states $T_i^{\pm}$ are composed of an X_i ($i = 2, 3$) exciton

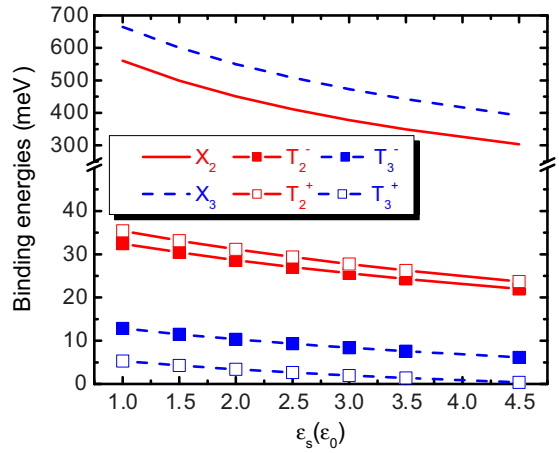

FIG. 4. Binding energies of neutral (X_i), positively (T_i^+, open symbols), and negatively (T_i^-, full symbols) charged excitons ($i = 2, 3$) in monolayer TiS_3 as a function of the relative permittivity of the substrate medium.

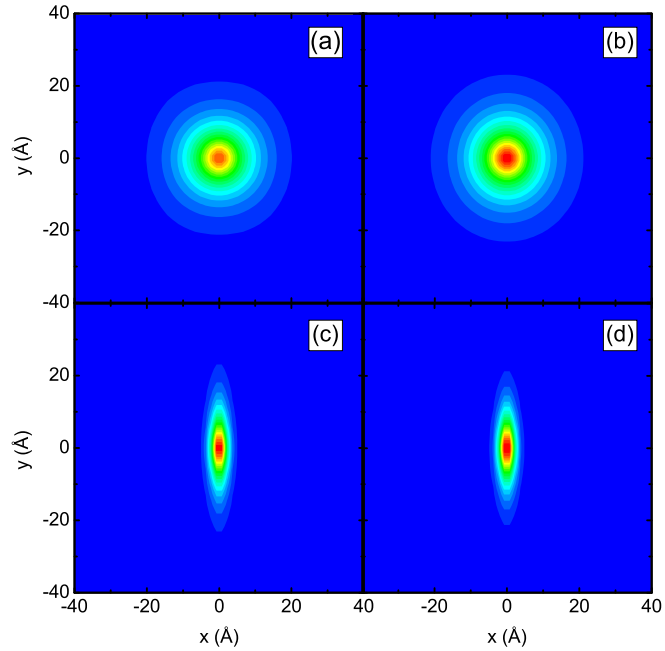

FIG. 5. Correlation function $g_{e\text{-}h}$ between the first electron and hole for (a,c) positively and (b,d) negatively charged trions. The upper (lower) row is for $T^{\pm}_{2(3)}$ trions.

with an additional electron (hole), represented by the $-$ $(+)$ superscript, which is assumed to be always in the minimum (maximum) of the conduction (valence) band, even when the charge carriers in the exciton are in a higher (lower) band (as is the case for electrons in X_2 and both charge carriers in X_3; see Fig. 2). Notice that the trion Hamiltonian (5) is exact, as long as one assumes that the quasi-particle bands obtained by DFT are not significantly modified by the interaction between charged particles, which is just the usual approximation behind the Wannier-Mott framework. In other words, a trion Hamiltonian written in such a basis composed of $T_2^{\pm}$ and $T_3^{\pm}$ states is expected to have negligibly small coupling between the bands involved in the excitonic transitions, which is a reasonable approximation, as these trion energies are relatively far from each other in energy. Besides, X_2 and X_3 states are obtained with different polarization directions, as previously discussed, therefore, binding energies of $T_2^{\pm}$ and $T_3^{\pm}$ trions are more conveniently calculated and are discussed separately. Trion binding energies are observed to be tens of meV, similar to those of monolayer TMDCs [59,61] and black phosphorus [50], except for T_3^+. Positive and negative trions have significantly different binding energies, especially for $T_3^{\pm}$ ($\approx$8 meV), which can be experimentally verified by checking the trion peak position as a function of the doping of the TiS_3 monolayer. In fact, as the dielectric constant of the substrate increases, the positive trion T_3^+ becomes weakly bound, with very low binding energy. Notice that, for $T_2^{\pm}$, it is T_2^- that is less energetic.

Differences between positive and negative trion energies are related to the difference between effective masses of electrons and holes [62]. Moreover, the opposite behavior observed for $T_2^{\pm}$ as compared to $T_3^{\pm}$ is a consequence of the different band anisotropy axis, which affects the single-particle effective masses involved. As previously mentioned, the electron band is the same for both X_2 and X_3 ($m_e^x = 12.07m_0$, $m_e^y = 0.42m_0$). In the $T_2^{\pm}$ case, we start with an X_2 exciton, whose hole band exhibits anisotropy axis perpendicular to that of the electron band ($m_h^x = 0.36m_0$, $m_h^y = 0.90m_0$). Conversely, for $T_3^{\pm}$, we have an X_3 exciton whose hole band is qualitatively similar to that of the electron ($m_h^x = 50m_0$ and $m_h^y = 0.25m_0$). The third particle, in both cases, is then either an electron in the lowest conduction band ($\bar{m}_e^x = 1.54m_0$, $\bar{m}_e^y = 0.46m_0$) or a hole in the highest valence band ($\bar{m}_h^x = 0.36m_0$, $\bar{m}_h^y = 0.90m_0$).

In order to investigate the effect of such interplay between effective mass anisotropies of conduction and valence bands in $T_2^{\pm}$ and $T_3^{\pm}$ trion states, we analyze, for each case, the correlation functions

$$g_{e\text{-}h}(\vec{\rho}) = \langle \delta(\vec{\rho} - \vec{R}) \rangle = \int_{S_r} |\Psi(\vec{r}, \vec{\rho})| d^2 r, \tag{8}$$

between the electron and hole that compose the exciton, and

$$g_{c\text{-}c.m.}(\vec{\rho}) = \langle \delta(\vec{\rho} - \vec{r}) \rangle = \int_{S_R} |\Psi(\vec{\rho}, \vec{R})| d^2 R, \tag{9}$$

between the third charge and the exciton center of mass, where $|\Psi(\vec{r}, \vec{R})|$ is the trion ground state wave function for the Hamiltonian (5). The resulting color plot map of the exciton correlation function $g_{e\text{-}h}(\vec{\rho})$ is shown in Figs. 5(a) and 5(b), for T_2^+ and T_2^-, and Figs. 5(c) and 5(d), for T_3^+ and T_3^-, respectively. The consistently perpendicular anisotropy axis for both electrons (holes) and the hole (electron) in $T_2^{-(+)}$ makes the excitonic pair contribution to the trion more circularly symmetric, even when compared to other anisotropic systems, such as monolayer black phosphorus [50]. On the other hand, for T_3^-, both electrons and the hole share the same anisotropy axis, thus leading to an exciton correlation function that is strongly squeezed in the x direction. Even though the second hole in T_3^- has its effective mass anisotropy axis perpendicular to that of the electron and the first hole in this trion, it is not enough to equilibrate the exciton correlation function anisotropy, which is still qualitatively similar to that

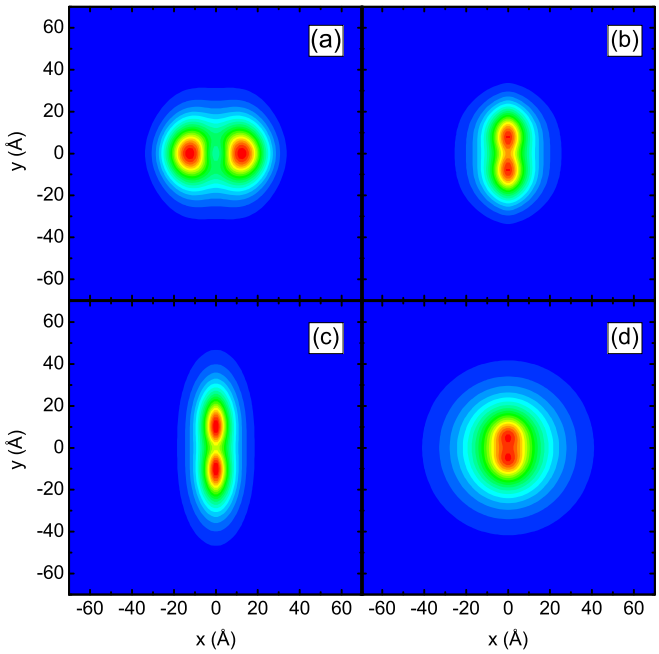

FIG. 6. Correlation function $g_{c\text{-}c.m.}$ between the third charge and the exciton center of mass for (a,c) positively and (b,d) negatively charged trions. The upper (lower) row is for $T^{\pm}_{2(3)}$ trions.

of the T_3^+ trion. As a consequence, $g_{e\text{-}h}(\vec{\rho})$ for each trion state is not significantly different for the different extra charges and, although not shown here, it is also qualitatively similar to the wave functions of the X_2 and X_3 excitons themselves. However, the sign of the charge of the third particle in the trion strongly determines its correlation $g_{c\text{-}c.m.}(\vec{\rho})$ with the exciton center of mass: Figs. 6(a) and 6(b), for T_2^+ and T_2^-, respectively, show $g_{c\text{-}c.m.}(\vec{\rho})$ stretched along different directions. Indeed, the probability density for the third particle with respect to the exciton center of mass must exhibit a peak at a certain distance from the origin, since this particle is attracted by one of the charges composing the exciton, but repelled by the other. In an isotropic system, the third particle could be anywhere at some distance to the origin, so that its correlation function has a ring shape [50]. However, in such an anisotropic system, it must lie in the direction where the effective mass is lighter. This is verified by the fact that $g_{c\text{-}c.m.}(\vec{\rho})$ exhibits peaks in the $x(y)$ direction when the third charge is positive (negative). As for T_3^+ and T_3^-, the $g_{c\text{-}c.m.}(\vec{\rho})$ respectively shown in Figs. 6(c) and 6(d) exhibit peaks in the same direction. This is a consequence of the fact that even though the extra hole in T_3^+ has its effective mass anisotropy axis perpendicular to that of the electron, there is still a much heavier hole in this trion whose anisotropy axis is in the same direction as the one of the electron, thus stretching $g_{c\text{-}c.m.}(\vec{\rho})$ in the same direction for both T_3^+ and T_3^-.

III. CONCLUSIONS

The absorption spectra for different light polarization directions exhibit very different excitonic peak features if the compound exhibits reduced in-plane structural symmetry. In contrast with one of the most prominent anisotropic 2D materials, namely few-layer BP, interband transitions for light polarized in the zigzag direction of TiS_3 are allowed, but rather exhibit peaks at different energies. Exciton binding energies found in the BSE step are in good agreement with those obtained by effective mass theory for a planar Wannier exciton with electrons and holes interacting via the Rytova-Keldysh potential. Within this model, we are also able to calculate trion binding energies, which are shown to be significantly different for the positively and negatively charged cases, and to exhibit anisotropic probability density distributions. The strikingly different physical properties of excitons and trions excited by light with different polarization directions render monolayer TiS_3 a highly tunable material for future optoelectronic applications.

ACKNOWLEDGMENTS

This work was supported by the Flemish Science Foundation (FWO-Vl) and the FLAG-ERA project TRANS-2D-TMD. H.S. acknowledges financial support from TUBITAK under Project No. 117F095. A.C. acknowledges support from the Brazilian Research Council (CNPq), through the PRONEX/FUNCAP and Science Without Borders programs, and from the Lemann Foundation. E.T. and L.W. acknowledge support from the National Research Fund, Luxembourg (INTER/ANR/13/20/NANOTMD).

[1] K. S. Novoselov, A. K. Geim, S. V. Morozov, D. Jiang, Y. Zhang, S. V. Dubonos, I. V. Grigorieva, and A. A. Firsov, Science **306**, 666 (2004).
[2] A. K. Geim and K. S. Novoselov, Nat. Mater. **6**, 183 (2007).
[3] K. Wu, E. Torun, H. Sahin, B. Chen, X. Fan, A. Pant, D. P. Wright, T. Aoki, F. M. Peeters, E. Soignard, and S. Tongay, Nat. Commun. **7**, 12952 (2016).
[4] A. Pant, E. Torun, B. Chen, S. Bhat, X. Fan, K. Wu, D. P. Wright, F. M. Peeters, E. Soignard, H. Sahin, and S. Tongay, Nanoscale **8**, 16259 (2016).
[5] J. O. Island, M. Buscema, M. Barawi, J. M. Clamagirand, J. R. Ares, C. Sánchez, I. J. Ferrer, G. A. Steele, H. S. J. van der Zant, and A. Castellanos-Gomez, Adv. Opt. Mater. **2**, 641 (2014).
[6] Q. H. Wang, K. Kalantar-Zadeh, A. Kis, J. N. Coleman, and M. S. Strano, Nat. Nanotechnol. **7**, 699 (2012).
[7] B. Radisavljevic, A. Radenovic, J. Brivio, V. Giacometti, and A. Kis, Nat. Nanotechnol. **6**, 147 (2012).
[8] M. Chhowalla, Nat. Chem. **5**, 263 (2013).
[9] K. C. Santosh, C. Zhang, S. Hong, R. M. Wallace, and K. Cho, 2D Mater. **2**, 035019 (2015).
[10] L. Brattas and A. Kjekshus, Acta Chem. Scand. **26**, 3441 (1972).
[11] S. Furuseth, L. Brattas, and A. Kjekshus, Acta Chem. Scand. **29a**, 623 (1975).
[12] E. Liu, Y. Fu, Y. Wang, Y. Feng, H. Liu, X. Wan, W. Zhou, B. Wang, L. Shao, and C.-H. Ho, Nat. Commun. **6**, 6991 (2015).
[13] K. Sasagawa, S. Shishido, K. Ando, H. Matsuoka, T. Noda, T. Tokuda, K. Kakiuchi, and J. Ohta, Opt. Express **21**, 11132 (2013).
[14] S. Shishido, T. Noda, K. Sasagawa, T. Tokuda, and J. Ohta, Jpn. J. Appl. Phys. **50**, 04DL01 (2011).

[15] Y.-L. Liao and Y. Zhao, Opt. Quantum Electron. **46**, 641 (2014).
[16] M. Guillaumée, L. Dunbar, C. Santschi, E. Grenet, R. Eckert, O. Martin, and R. Stanley, Appl. Phys. Lett. **94**, 193503 (2009).
[17] H. Yuan, X. Liu, F. Afshinmanesh, W. Li, G. Xu, J. Sun, B. Lian, A. G. Curto, G. Ye, and Y. Hikita, Nat. Nano **10**, 707 (2015).
[18] E. Zhang, P. Wang, Z. Li, H. Wang, C. Song, C. Huang, Z.-G. Chen, L. Yang, K. Zhang, and S. Lu, ACS Nano **10**, 8067 (2016).
[19] S. Nanot, A. W. Cummings, C. L. Pint, A. Ikeuchi, T. Akiho, K. Sueoka, R. H. Hauge, F. Leonard, and J. Kano, Sci. Rep. **3**, 1335 (2013).
[20] E. Matioli, S. Brinkley, K. M. Kelchner, Y.-L. Hu, S. Nakamura, S. Den Baars, J. Speck, and C. Weisbuch, Light: Sci. Appl. **1**, e22 (2012).
[21] S. B. Singer, M. Mecklenburg, E. R. White, and B. C. Regan, Phys. Rev. B **83**, 233404 (2011).
[22] J. Liu, Y. Guo, F. Q. Wang, and Q. Wang, Nanoscale **10**, 807 (2018).
[23] I. J. Ferrer, J. R. Ares, J. M. Clamagirand, M. Barawi, and C. Sanchez, Thin Solid Films **535**, 398 (2012).
[24] A. J. Molina-Mendoza, M. Barawi, R. Biele, E. Flores, J. R. Arse, C. Sanchez, G. Rubio-Bollinnger, N. Agrait, R. D'Agosta, I. J. Ferrer, and A. Castellanos-Gomez, Adv. Electron. Mater. **1**, 1500126 (2015).
[25] J. O. Island, M. Barawi, R. Biele, A. Almazan, J. M. Clamagirand, J. R. Ares, C. Sanchez, H. S. van der Zant, J. V. Alvarez, R. D'Agosta, I. J. Ferrer, and A. Castellanos-Gomez, Adv. Mater. **27**, 2595 (2015).
[26] J. Kang and L.-W. Wang, Phys. Chem. Chem. Phys. **18**, 14805 (2016).
[27] R. Biele, E. Flores, J. R. Ares, C. Sanchez, I. J. Ferrer, G. Rubio-Bollinger, A. Castellanos-Gomez, and R. D'Agosta, Nano Research **11**, 225 (2018).
[28] J. Dai and X. C. Zeng, Angew. Chem. **54**, 7572 (2015).
[29] I. G. Gorlova, V. Y. Pokrovskii, S. G. Zybtsev, A. N. Titov, and V. N. Timofeev, J. Exp. Theor. Phys. **111**, 298 (2010).
[30] P. Giannozzi, S. Baroni, N. Bonini, M. Calandra, R. Car, C. Cavazzoni, D. Ceresoli, G. L. Chiarotti, M. Cococcioni, I. Dabo, A. Dal Corso, S. de Gironcoli, S. Fabris, G. Fratesi, R. Gebauer, U. Gerstmann, C. Gougoussis, A. Kokalj, M. Lazzeri, L. Martin-Samos, N. Marzari, F. Mauri, R. Mazzarello, S. Paolini, A. Pasquarello, L. Paulatto, C. Sbraccia, S. Scandolo, G. Sclauzero, A. P. Seitsonen, A. Smogunov, P. Umari, and R. M. Wentzcovitch, J. Phys.: Condens. Matter **21**, 395502 (2009).
[31] J. P. Perdew, K. Burke, and M. Ernzerhof, Phys. Rev. Lett. **78**, 1396 (1997).
[32] C. Hartwigsen, S. Goedecker, and J. Hutter, Phys. Rev. B **58**, 3641 (1998).
[33] S. Goedecker, M. Teter, and J. Hutter, Phys. Rev. B **54**, 1703 (1996).
[34] G. Onida, L. Reining, and A. Rubio, Rev. Mod. Phys. **74**, 601 (2002).
[35] L. Hedin and S. Lundqvist, Solid State Phys. **23**, 1 (1970).
[36] A. Marini, C. Hogan, M. Grüning, and D. Varsano, Comput. Phys. Commun. **180**, 1392 (2009).
[37] G. Strinati, Phys. Rev. Lett. **49**, 1519 (1982).
[38] M. Rohlfing and S. G. Louie, Phys. Rev. B **62**, 4927 (2000).
[39] M. Palummo, O. Pulci, R. D. Sole, A. Marini, P. Hahn, W. G. Schmidt, and F. Bechstedt, J. Phys.: Condens. Matter **16**, S4313 (2004).
[40] F. Iyikanat, H. Sahin, R. T. Senger, and F. M. Peeters, J. Phys. Chem. C **119**, 10709 (2015).
[41] Y. Aierken, D. Çakır, and F. M. Peeters, Phys. Chem. Chem. Phys. **18**, 14434 (2016).
[42] J. O. Island, A. J. Molina-Mendoza, M. Barawi, R. Biele, E. Flores, J. M. Clamagirand, J. R. Ares, C. Sanchez, H. S. J. van der Zant, R. D'Agosta, I. J. Ferrer, and Andres Castellanos-Gomez, 2D Mater. **4**, 022003 (2017).
[43] J. O. Island, R. Biele, M. Barawi, J. M. Clamagirand, J. R. Ares, C. Sanchez, H. S. J. van der Zant, I. J. Ferrer, R. D'Agosta, and A. Castellanos-Gomez, Sci. Rep. **6**, 22214 (2016).
[44] A. Chaves, T. Low, P. Avouris, D. Çakır, and F. M. Peeters, Phys. Rev. B **91**, 155311 (2015).
[45] N. S. Rytova, Proc. MSU, Phys. Astron. **3**, 30 (1967).
[46] L. V. Keldysh, JETP Lett. **29**, 658 (1979).
[47] T. Galvani, F. Paleari, H. P. C. Miranda, A. Molina-Sánchez, L. Wirtz, S. Latil, H. Amara, and F. Ducastelle, Phys. Rev. B **94**, 125303 (2016).
[48] P. Cudazzo, I. V. Tokatly, and A. Rubio, Phys. Rev. B **84**, 085406 (2011).
[49] L. D. Landau and E. M. Lifshitz, *Electrodynamics of Continuous Media* (Pergamon, Oxford, 1960), p. 61.
[50] A. Chaves, M. Z. Mayers, F. M. Peeters, and D. R. Reichman, Phys. Rev. B **93**, 115314 (2016).
[51] M. H. Degani and M. Z. Maialle, J. Comput. Theor. Nanosci. **7**, 454 (2010).
[52] A. Chaves, G. A. Farias, F. M. Peeters, and R. Ferreira, Commun. Comput. Phys. **17**, 850 (2015).
[53] M. Suzuki, Phys. Lett. A **165**, 387 (1992).
[54] T. C. Berkelbach, M. S. Hybertsen, and D. R. Reichman, Phys. Rev. B **88**, 045318 (2013).
[55] A. Chernikov, T. C. Berkelbach, H. M. Hill, A. Rigosi, Y. Li, O. B. Aslan, D. R. Reichman, M. S. Hybertsen, and T. F. Heinz, Phys. Rev. Lett. **113**, 076802 (2014).
[56] A. Molina-Sánchez, K. Hummer, and L. Wirtz, Surf. Sci. Rep. **70**, 554 (2015).
[57] A. Molina-Sánchez, D. Sangalli, K. Hummer, A. Marini, and L. Wirtz, Phys. Rev. B **88**, 045412 (2013).
[58] E. Torun, H. P. C. Miranda, A. Molina-Sánchez, and Ludger Wirtz, Phys. Rev. B **97**, 245427 (2018).
[59] T. Low, A. Chaves, J. D. Caldwell, A. Kumar, N. X. Fang, P. Avouris, T. F. Heinz, F. Guinea, L. Martin-Moreno, and F. Koppens, Nat. Mater. **16**, 182 (2017).
[60] K. He, N. Kumar, L. Zhao, Z. Wang, K. F. Mak, H. Zhao, and J. Shan, Phys. Rev. Lett. **113**, 026803 (2014).
[61] M. Z. Mayers, T. C. Berkelbach, M. S. Hybertsen, and D. R. Reichman, Phys. Rev. B **92**, 161404(R) (2015).
[62] I. Filikhin, R. Ya. Kezerashvili, and B. Vlahovic, Phys. Lett. A **382**, 787 (2017).